New Fluorinated Dithienyl-Diketopyrrolopyrrole Monomers and Polymers for Organic Electronics

Thomas Bura[1], Serge Beaupré[1], Olzhas A. Ibraikulov[2], Marc-André Légaré[3], Jesse Quinn[4], Patrick Lévêque[2], Thomas Heiser[2], Yuning Li[4], Nicolas Leclerc[5], Mario Leclerc[1,*]

T. Bura and S. Beaupré contributed equally

1) Canada Research Chair on Electroactive and Photoactive Polymers, Department of Chemistry, Université Laval, Quebec City, Quebec, G1V 0A6 (Canada)

2) Laboratoire ICube, DESSP, Université de Strasbourg, CNRS, 23 rue du Loess, Strasbourg, 67037 (France)

3) Institut für Anorganische Chemie, Julius-Maximilians Universität Würzburg, Am Hubland, Würzburg, 97074 (Germany)

4) Department of Chemical Engineering, University of Waterloo, Waterloo, Ontario, N2L 3G1 (Canada)

5) Institut de Chimie et Procédés pour l'Énergie, l'Environnement et la Santé, ICPEES, Université de Strasbourg, CNRS, Strasbourg, 67087 (France)

E-mail : Mario.Leclerc@chm.ulaval.ca

TOC

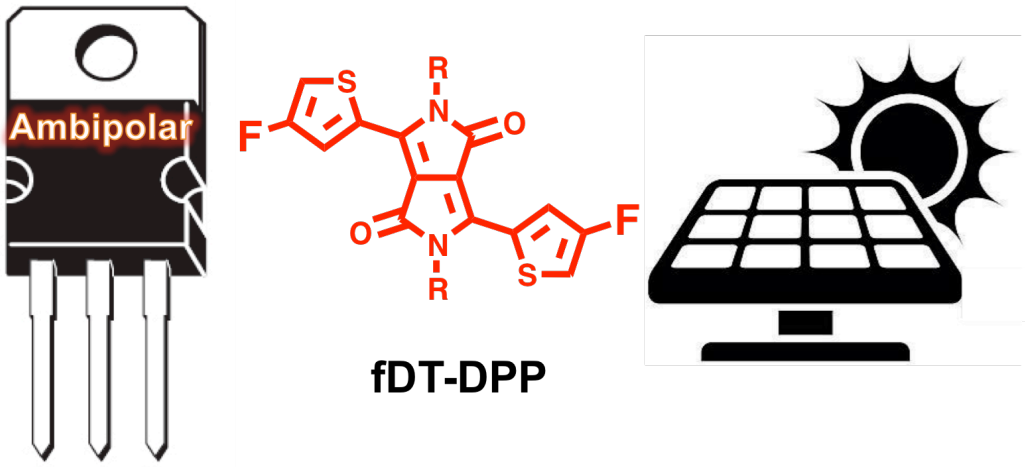

Abstract

Diketopyrrolopyrrole (DPP) derivatives are among the most efficient materials studied for both polymer solar cell (PSC) and organic field-effect transistor (OFET) applications. We report here the synthesis of new fluorinated dithienyl-diketopyrrolopyrrole (fDT-DPP) monomers suitable for direct heteroarylation polymerization. fDT-DPP-based copolymers were then prepared to probe the effect of the fluorination. It was found that they feature deeper HOMO energy levels and smaller bandgaps than their non-fluorinated analogues. Moreover, some fDT-DPP copolymers show ambipolar behavior when tested in OFETs. For example, **P2** shows hole mobility up to 0.8 $cm^2 V^{-1} s^{-1}$ and electron mobility up to 0.5 $cm^2 V^{-1} s^{-1}$. Inverted PSCs with power conversion efficiency (PCE) up to 7.42% was also obtained for **P5.** These results reported here (OFETs and PSCs) confirm that the fluorination of dithienyl-DPP moieties improves the performance of organic electronics devices. This study is also evidencing the strength of the direct heteroarylation polymerization and fDT-DPP as a new class of conjugated polymers.

1. Introduction

In the past few years, organic solar cells (OSCs) and organic field-effect transistors (OFETs) based on π-conjugated polymers have stimulated broad interest from academic and industrial laboratories due to the possibility of creating efficient, lightweight and flexible devices using inexpensive and environmentally friendly solution-based printing techniques [1-6]. Tuning of the physical and electro-optical properties of conjugated polymers through chemical modification of their backbone has led to a wide array of promising materials for organic electronics applications. Indeed, with polymer solar cells (PSC) exhibiting power conversion efficiency (PCE) exceeding 10% [7-10], OFETs with hole mobility up to 20 $cm^2 V^{-1} s^{-1}$ [11] and electron mobility as high as 7.0 $cm^2 V^{-1} s^{-1}$[12], conjugated polymers now show performance suitable for commercial applications. Among all the new electroactive and photoactive materials developed over the past 20 years, 2,5-dihydropyrrolo[3,4-*c*]pyrrole-1,4-dione (DPP) based polymers have been found especially valuable since they deliver high efficiencies in both PSCs and OFETs. For example, PDPPTT, a copolymer made from dithienyl-DPP and thieno[3,2-*b*]thiophene (TT) showed PCE up to 9.4% [13] and hole mobility up to 10.5 $cm^2 V^{-1} s^{-1}$[14]. Since the first report on the synthesis of 3,6-diphenyl-DPP by Farnum *et al*. in 1974 [15], the synthesis and the modulation of the electro-optical properties DPP copolymers have been extensively studied and reviewed [16-27]. The flanking aromatic substituents (five- or six-membered-fused or unfused heterocyclic rings) strongly modulate the electro-optical properties. Flanking thiophenes, a five-membered ring, notably have minimal steric effects on the DPP core and lead to coplanar dithienyl-DPP building blocks that are widely used in conjugated polymers. Recently, fluorination of conjugated backbone of D-A copolymers has proven to be effective to enhance the performance of PSC and OFETs [28]. The strong

electronegativity of fluorine effectively lowers both the HOMO and LUMO energy levels of the fluorinated copolymers without perturbing the planarity of the backbone, thanks to its small van der Waals radius (r = 0.135 nm). In addition, changes in crystallinity, internal polarization and morphology of the active layer have also been attributed to fluorination. Up to now, the best-performing semiconducting polymers incorporate fluorine atoms in their chemical structure [29-33]. It is then believed that fluorinated dithienyl-DPP-based polymers are capable to exhibit ambipolarity in OFETs, which is specifically attractive for the fabrication of single-semiconductor complementary metal-oxide-semiconductor (CMOS) inverters and light emitting devices [34-40]. A single organic semiconductor would facilitate the fabrication of CMOS-inverters and the devices are much more stable in comparison to the semiconductor blends and/or double-layer semiconductor films, which have demonstrated difficulties related to nanomorphological formation in the blended films or coalescing of the bilayers [41]. Ambipolar polymers based on electron acceptors of naphthalene diimide (NDI) [42-45], benzodifurandione [46-49], isoindigo (IID) [50-52], and diketopyrrolopyrrole (DPP) [53-60] or its derivatives [61,62] have been reported; however, there are still only a small number of polymeric semiconductors that display ambipolar characteristics with high and balanced hole and electron mobilities [63].

Along these lines, we report for the first time an efficient and reliable procedure for the synthesis of pure 4-fluoro-2-thiophenecarbonitrile, a pivotal component for the synthesis of fluorinated dithieno-diketopyrrolopyrrole (fDT-DPP) (Scheme 1). Unlike the work reported by by Jiang *et al.* on fluoro-diphenyl-DPP (fDP-DPP) [64], we found that the synthesis of fDT-DPP proceeded smoothly using the well-established

succinate-based procedure. fDT-DPP-based copolymers, prepared by direct (hetero)arylation polymerization exhibit broad and red shifted absorption in the UV-vis-NIR region with deeper HOMO energy levels compared to their non-fluorinated analogues. When tested in OFETs, a fDT-DPP polymer shows an ambipolar behavior with both high hole and electron mobilities whereas other copolymers demonstrated highly interesting photovoltaic properties. Based on these results, fDT-DPP is clearly a promising building block for organic electronics.

2. Experimental

2.1 Methods

^{1}H, ^{13}C and ^{19}F NMR spectra were recorded on a Varian AS400 or Agilent DD2 500MHz apparatus in deuterated solvents. Chemical shifts were reported as δ values (ppm) relative to the residual protic solvent. The number-average ($\overline{M_n}$) and weight-average ($\overline{M_w}$) molecular weights were determined by size exclusion chromatography (SEC) using a Malvern HT-GPC equipped with an RI detector. The flow rate was fixed at 0.75 mL/min using 1,2,4-trichlorobenzene (TCB) (with 0.0125% BHT w/v) as the eluent. The temperature of the system was set to 140 °C. All the samples were prepared at concentrations of nominally 0.50 mg/mL in TCB. The sample vials were held at 140 °C with stirring for 1 h for complete dissolution. The calibration method used to generate the reported data was the classical polystyrene method using polystyrene standards which were dissolved in TCB. UV-Vis absorption spectra were taken using a Thermo Scientific Genesys 10S spectrophotometer using 1 cm path-length quartz cells. For solid-state measurements, polymer solution was spun-cast on glass plates. Optical bandgaps were calculated from the onset of the absorption band. Cyclic voltammograms were recorded on a Solartron 1287 potentiostat using platinum wires

as working electrode and counter-electrode at a scan rate of 50 mV/s. The reference electrode was Ag/Ag^+ (0.01 M of $AgNO_3$ in acetonitrile) and the electrolyte was a solution of 0.1 M of tetrabutylammonium hexafluorophosphate (Bu_4NPF_6) in dry acetonitrile. In these conditions, the oxidation potential of Ferrocene was 0.09 V versus Ag/Ag+, whereas the oxidation potential of Ferrocene was 0.41 V versus saturated calomel electrode (SCE). The HOMO and LUMO energy levels were determined from the oxidation and reduction onsets (where the current differs from the baseline) assuming that SCE electrode is –4.71 eV from vacuum, as reported in the literature [65]. Thermogravimetric analysis (TGA) measurements were carried out with a Mettler Toledo TGA SDTA 851e apparatus at a heating rate of 10 ºC /min under a nitrogen atmosphere. The temperature of degradation (T_d) corresponds to a 5% weight loss. Differential scanning calorimetry (DSC) analyses were performed on a Perkin-Elmer DSC-7 instrument calibrated with ultrapure indium at a scanning rate of 10 ºC/min under a nitrogen flow. The WAXS diffraction (powder) measurements were done with a Krytalloflex 760 generator (40kV, 40mA), a goniometer and a two-dimensional Hi-Star detector. A sealed tube emitting at 1.5418 Å (copper Kα) nickel-filtered was used as the source. GADDS software was used to control and to perform analysis of all experiments.

2.2 Fabrication and Testing of OFETs

Organic field effect transistors (OFETs) were fabricated on a heavily n^{++}-doped Si/SiO_2 substrate with bottom-contact bottom-gate configuration (BGBC). The thermal grown SiO_2 (~300 nm) was used as the gate dielectric and the conductive Si layer functioned as the gate. The gold source/drain contact pairs with a channel length of 30 μm and a channel width of 1000 μm were obtained by conventional photolithography and thermal

deposition. The substrate was then plasma treated and cleaned by ultra-sonication with acetone, isopropanol, and dried with nitrogen and baked at 120 °C for 1 min. The substrate was then cooled to room temperature, dried, and submerged in a dodecyltrichlorosilane (DDTS) solution (3% in toluene) for 20 min and then rinsed with toluene and dried with nitrogen. Subsequently, a polymer layer was deposited by spin-coating a polymer solution in *o*-dichlorobenzene (*o*-DCB) (10 mg mL^{-1}) at 3000 rpm for 80 s in a glove box. After annealing at a pre-determined temperature in the glove box filled with nitrogen for 20 min, the devices were characterized in the same glove box with an Agilent B2912A Semiconductor Analyzer. The mobility in the saturation region was calculated according to the following equation:

$$I_{DS} = \frac{W}{2L} C_i \mu (V_{GS} - V_{TH})^2$$

where I_{DS} is the drain current, W and L are the device channel width and length, C_i is the gate dielectric layer capacitance per unit area (~11.6 nF cm^{-2}), μ is the carrier mobility, V_{GS} and V_{TH} are gate voltage and threshold voltage.

2.3. Fabrication and testing of Hole-only Space Charge Limited Current Devices

ITO coated glass was utilized as a substrate. Substrates were cleaned consecutively in ultrasonic baths at 45°C for 15 min using soapsuds, acetone, and isopropanol and followed by 15 min UV-ozone treatment. A thin poly(ethylenedioxythiophene):polystyrene sulfonate (PEDOT:PSS) layer was spincoated onto pre-cleaned ITO and used as a bottom electrode. Polymer and polymer:fullerene layers were spincoated from hot solutions (≈ 110 °C) onto pre-heated substrates (≈ 110 °C). Devices were left overnight under high vacuum (≈ $5x10^{-7}$ mbar) and were completed by thermally evaporated MoO_3 (7 nm)/Ag (120 nm) layer. SCLC

diode (surface area: 1 mm^2) current-voltage characteristics were measured using a Keithley 4200 semiconductor characterization system.

2.4. Fabrication and testing of polymer solar cells.

ITO coated glass was utilized as a substrate. A ZnO layer (≈ 20-25 nm) was spincoated from ZnO nanoparticles solution (Nanograde N10) onto pre-cleaned ITO and thermally annealed at 100°C for 10 min and used as an electron extracting electrode. Active layers were elaborated from o-DCB and o-DCB/additive (DIO/DPE) solutions using blends of polymers and $PC_{71}BM$ as an electron acceptor material at various weight ratios. The concentrations of solutions were 8 mg/mL with respect to polymer content. Top electrode consisting of MoO_3 (7 nm)/Ag (120 nm) was thermally evaporated under ≈ $5x10^{-7}$ mbar vacuum. Four diodes with a 12 mm^2 active area were elaborated per substrate. All characterization was done in nitrogen atmosphere under dark and simulated AM1.5G standard irradiation (100 mW/cm^2, Lot Oriel Sun 3000 solar simulator).

2.5 Materials

2,3-Dibromothiophene (**1**) and N-Fluorobenzenesulfonimide (NFSI) were purchased from Combiblocks. NFSI recrystallized in diethyl ether prior to use. n-octyldimethylchlorosilane was purchased from Gelest Inc. **P1** [66], 2,7-Dibromo-9-(heptadecan-9-yl)-9H-carbazole (**M1**) [67], 3,6-Bis(thiophen-2-yl)-2,5-bis(decyl)pyrrolo[3,4-c]pyrrole-1,4-dione (**M2**) [68], 3,6-Bis(thiophen-2-yl)-2,5-bis(dodecyl)pyrrolo[3,4-c]pyrrole-1,4-dione (**M3**) [66], 3,6-Bis(5-bromothiophen-2-yl)-2,5-bis(2-octyldodecyl)pyrrolo[3,4-c]pyrrole-1,4)-dione (**M4**) [69], tris(2-

cycloheptyloxyphenyl)phosphine (BuraPhos) [70] were synthesized according to procedures reported in literature.

2.6 Synthesis of monomers

2.6.1 Synthesis of 3-bromo-2-(dimethyloctylsilyl)-thiophene (2).

Compound **1** (12.33 g, 50.96 mmol, 1.0 eq.) was placed in a dried round-bottom flask with a magnetic stirrer and purged on a Schlenk line. Anhydrous diethyl ether (100 ml) was added and the solution was cooled to -80 °C using an Et_2O/N_2 ice bath. Then, a solution of *n*-BuLi (2.5 M in hexanes, 20.4 mL, 50.96 mmol, 1 eq.) was added dropwise and the mixture was left to react for 20 min at -80°C. After this time, n-octyldimethylchlorosilane (13.5 mL, 56.05 mmol, 1.1 eq.) was added rapidly and the reaction mixture was allowed to warm to room temperature and reacted overnight. The reaction was quenched with a saturated solution of NH_4Cl and extracted three times with diethyl ether. The combined organic phases were washed with water and brine, dried over $MgSO_4$ and concentrated under reduced pressure. Purification was achieved by vacuum distillation (b.p. 110-115°C at 0.35 mmHg) affording the desired compound as colorless oil (Y = 85%). ^{1}H NMR 500 MHz ($CDCl_3$) δ (ppm): 7.45 (d, J = 4.8 Hz, 1H), 7.10 (d, J = 4.8 Hz, 1H), 1.34-1.25 (m, 12H), 0.91-0.86 (m, 5H), 0.38 (s, 6H). ^{13}C NMR 126 MHz ($CDCl_3$) δ (ppm): 133.9, 132.6, 130.8, 117.4, 33.5, 32.1, 29.4, 23.8, 22.8, 15.5, 14.3, -2.3.

2.6.2 Synthesis of 3-fluoro-2-(dimethyloctylsilyl)-thiophene (3).

3-Bromo-2-(dimethyloctylsilyl)-thiophene **(2)** (5.64 g, 16.9 mmol, 1.0 eq.) and TMEDA (2.8 mL, 1.1 eq.) was placed in a dried round-bottom flask with magnetic stirrer and was purged on a Schlenk line. Anhydrous THF (180 ml) was added and the solution was cooled to -100 °C in an Et_2O/N_2 bath. Freshly recrystallized NFSI (6.4 g, 20.3 mmol, 1.2 eq.) was solubilized in 60 mL anhydrous THF in another round-bottom flask under argon and was also cooled to -100 °C. *n*-BuLi (2.5 M in hexane, 2.8 mL, 17.75 mmol, 1.05 eq.) was added dropwise into the solution of **2**, which was left to react for 25 minutes at -100°C. The solution with NFSI was then rapidly added dropwise to the organolithium mixture via a cannula while maintaining the low temperature of both flasks (-100°C). The reaction mixture was allowed to warm to room temperature and was left to react overnight. The reaction was quenched with a saturated solution of NH_4Cl and extracted three times with hexanes. The combined organic phases were washed with water and brine, dried over $MgSO_4$ and concentrated under vacuum. Purification was achieved by silica gel column chromatography with hexanes as eluent affording the desired compound as colorless oil (Y = 65%). ^{1}H NMR 500 MHz (Acetone-d_6) δ (ppm): 7.66 (dd, J = 5.0 Hz, 2.9 Hz, 1H), 6.95 (dd, J = 5.0 Hz, 1.5 Hz, 1H), 1.40-1.27 (m, 12H), 0.87 (t, J = 7.0 Hz, 3H), 0.83-0.80 (m, 2H), 0.31 (s, 6H). ^{19}F NMR 470 MHz (Acetone-d_6) δ (ppm): -122.4. ^{13}C NMR 101 MHz ($CDCl_3$) δ (ppm): 163.7 (d, J = 255.4 Hz), 129.8 (d, J = 8.6 Hz), 118.2 (d, J = 31.3 Hz), 114.4 (d, J = 30.9), 33.5, 32.1, 29.4, 23.8, 22.8, 16.2, 14.3, -2.1

2.6.3 Synthesis of 4-fluoro-5-(dimethyloctylsilyl)-2-thiophenecarboxaldehyde (4)

Compound **3** (1.45g, 5.31 mmol, 1.0 eq.) was placed in a dried round-bottom flask with a magnetic stirrer and purged on a Schlenk line. Anhydrous THF (20 ml) was added and the solution was cooled to -78°C. Then, a solution of *n*-BuLi (2.5 M in hexanes,

2.35 mL, 5.84 mmol, 1.1 eq.) was added dropwise and the mixture was reacted for 20 min at -78°C. Then, anhydrous DMF (0.9 mL, 10.6 mmol, 2.0 eq.) was added and the reaction mixture was allowed to warm to room temperature and was left to react overnight. The reaction was quenched with a saturated solution of NH_4Cl and extracted three times with diethyl ether. The combined organic phases were washed with water and brine, dried over $MgSO_4$ and concentrated under reduced pressure. Purification was achieved by silica gel column chromatography (eluent: ethyl acetate/hexanes 10/90) affording the desired compound as colorless oil (Y = 80%). ^{1}H NMR 500 MHz ($CDCl_3$) δ (ppm): 9.80 (d, J = 0.4 Hz, 1H), 7.46 (d, J = 1.8 Hz, 1H), 1.34-1.24 (m, 12H), 0.87 (t, J = 7.0 Hz), 0.83-0.80 (m, 2H), 0.35 (d, J = 0.35 Hz 6H). ^{19}F NMR 470 MHz ($CDCl_3$) δ (ppm): -116.6. ^{13}C NMR 101 MHz ($CDCl_3$) δ (ppm): 181.7 (d, J = 2.0 Hz), 162.9 (d, J = 258.4 Hz), 144.9 (d, J = 4.7 Hz), 127.8 (d, J = 30.8 Hz), 124.4 (d, J = 28.7 Hz), 33.4, 32, 29.3, 23.6, 22.8, 15.7, -2.4

2.6.4 Synthesis of 4-fluoro-2-thiophenecarboxaldehyde (5)

Compound **4** (0.60 g, 1.99 mmol, 1.0 eq.) was placed in a round-bottom flask with a magnetic stirrer and dissolved in THF (2 mL). Then, a solution of an aqueous 2M HCl (1.1 mL, 1.1 eq.) was added and the mixture was cooled at 0°C. TBAF.$3H_2O$ (1 g, 3.2 mmol, 1.6 eq.) was added and the reaction mixture was allowed to warm to room temperature and monitored by TLC (eluent: pentane/diethyl ether 90/10). At the end of reaction (typically 1h), the crude mixture was poured on silica gel (eluent: pentane/diethyl ether 90/10) without work up to afford the titled compound as white solid (Y = 80%). ^{1}H NMR 500 MHz ($CDCl_3$) δ (ppm): 9.83 (d, J = 1.3 Hz, 1H), 7.50 (m, 1H), 7.19 (m, 1H). ^{19}F NMR 470 MHz ($CDCl_3$) δ (ppm): -125.1. ^{13}C NMR 101

MHz ($CDCl_3$) δ (ppm): 182.2 (d, J = 2.2 Hz), 158.1 (d, J = 262.2 Hz), 141.1 (d, J = 4.9 Hz), 124.3 (d, J = 24.4 Hz), 113.9 (d, J = 20.6 Hz).

2.6.5 Synthesis of 4-fluoro-2-thiophenecarbonitrile (6)

Compound **5** (0.56 g, 4.31 mmol, 1.0 eq.) was placed in a round-bottom flask with a magnetic stirrer and then dissolved in NMP (2ml). Hydroxylamine hydrochloride (0.36 g, 5.17 mmol, 1.2 eq.) was added to the solution and the mixture was heated at 145°C until complete consumption of starting material (typically 3h). At the end of reaction, the crude mixture was poured on silica gel (eluent: pentane/diethyl ether 90/10) without work up to afford the desired compound as white solid (Y = 80%). ^{1}H NMR 400 MHz ($CDCl_3$) δ (ppm): 7.37 (dd, J = 1.7, 0.8 Hz, 1H), 7.04 (dd, J = 1.7, 1.1 Hz, 1H). ^{19}F NMR 470 MHz ($CDCl_3$) δ (ppm): -125.9. ^{13}C NMR 126 MHz ($CDCl_3$) δ (ppm): 156.9 (d, J = 261.5 Hz), 126.5 (d, J = 27.1 Hz), 113.4, 111.5 (d, J = 20.9 Hz), 109.3 (d, J = 10.9 Hz).

2.6.6 Synthesis of 3,6-(4-fluorothiophen-2-yl)pyrrolo[3,4-c]pyrrole-1,4-dione (7)

In a two neck flask equipped with a condenser and an addition funnel, sodium was added in 100 mL of 2-methyl-2-butanol and the mixture was heated at 105°C until complete consumption of sodium. Then, 4-fluoro-2-thiophenecarbonitrile (**6**) dissolved in 5 mL of 2-methyl-2-butanol was rapidly added into the mixture and diisopropyl succinate was slowly added through the addition funnel. The reaction mixture quickly turned purple. The reaction mixture was stirred overnight at 105°C. The reaction was cooled at 65 °C quenched by an addition of a mixture of methanol and acetic acid followed by heating at 90°C for 30 min. Then, the reaction mixture was allowed to cool to room temperature, filtered on Buchner and washed with methanol (Y = 75%). ^{1}H

NMR 400 MHz (DMSO) δ (ppm): 11.33 (s, 2H), 8.00 (d, J = 1.8 Hz, 2H), 7.65 (d, J = 1.5 Hz, 2H). ^{19}F NMR 376 MHz (DMSO) δ (ppm): -127.1. ^{13}C NMR 101 MHz (DMSO) δ (ppm): 161.4, 157 (d, J = 256.5 Hz), 136.2, 129.2 (d, J = 9.8 Hz), 119.3 (d, J = 27.5 Hz), 111.4 (d, J = 21.2 Hz), 109.4.

2.6.7 Synthesis of 3,6-(4-fluorothiophen-2-yl)-2,5-Bis(decyl)pyrrolo[3,4-c]pyrrole-1,4-dione (M5). In a two neck flask equipped with a condenser and an addition funnel, compound **7** (0.51 g, 1.51 mmol, 1.0 eq.) and anhydrous potassium carbonate (1 g, 4.55 mmol, 3 eq.) were stirred in 8 mL of anhydrous DMF. The mixture was heated at 85°C for 30 min and then 1-bromodecane (0.632 g, 4.55 mmol, 3.0 eq.) was slowly added. The reaction mixture was stirred overnight at 85°C. After cooling to room temperature, the reaction was quenched with a saturated solution of NH_4Cl and extracted three times with diethyl ether. The combined organic phases were washed with water and brine, dried over $MgSO_4$ and concentrated under reduced pressure. Purification was achieved by silica gel column chromatography (eluent: chloroform/hexanes 65/35) affording the desired compound as purple solid (Y = 40%). ^{1}H NMR 500 MHz ($CDCl_3$) δ (ppm): 8.70 (d, J = 1.7 Hz, 2H), 7.04 (dd, J = 1.6, 0.5 Hz, 2H), 4.05-4.01 (m, 4H), 1.76-1.70 (m, 4H), 1.43-1.25 (m, 28H), 0.87 (t, J = 7 Hz, 6H). ^{19}F NMR 470 MHz ($CDCl_3$) δ (ppm): -126. ^{13}C NMR 101 MHz ($CDCl_3$) δ (ppm): 161.1, 158.7 (d, J = 260.3 Hz), 139.5 (d, J = 3.2 Hz), 128.2 (d, J = 9.3 Hz), 123.9 (d, J = 27.6 Hz), 109.3 (d, J = 21.4 Hz), 108.3, 42.4, 32, 30.1, 29.6, 29.4, 29.3, 27, 22.8, 14.3.

2.6.8. Synthesis of 3,6-(4-fluorothiophen-2-yl)-2,5-Bis(dodecyl)pyrrolo[3,4-c]pyrrole-1,4-dione (M6). M6 was synthetized and purified according to the procedure described for **M5** using 1-bromododecane instead of 1-bromodecane affording the desired compound as purple solid (Y = 43%). ^{1}H NMR 500 MHz ($CDCl_3$) δ (ppm): 8.69 (d, J = 1.7 Hz, 2H), 7.04 (dd, J = 1.6, 0.5 Hz, 2H), 4.05-4.01 (m, 4H), 1.77-1.69 (m, 4H), 1.40-1.25 (m, 36H), 0.87 (t, J = 7 Hz, 6H). ^{19}F NMR 376 MHz ($CDCl_3$) δ (ppm): -126. ^{13}C NMR 101 MHz ($CDCl_3$) δ (ppm): 161.1, 158.7 (d, J = 260.2 Hz), 139.5 (d, J = 3.0 Hz), 128.2 (d, J = 9.4 Hz), 123.9 (d, J = 27.5 Hz), 109.3 (d, J = 21.5 Hz), 108.3, 42.4, 32.1, 30.1, 29.8, 29.7, 29.6, 29.5, 29.4, 27, 22.8, 14.3.

2.7 Synthesis of polymers by direct heteroarylation polymerization (DHAP)

2.7.1 Synthesis of P2: M6 (0.082 mmol, 1.0 eq.), **M4** (0.082 mmol, 1.0 eq.), *trans*-Bis(acetato)bis[o-(di-o-tolylphosphino)benzyl]dipalladium(II) (2 % mol), tris(2-methoxyphenyl)phosphine (8 % mol), Cs_2CO_3 (3 eq.) and pivalic acid (1 eq.) were put in a microwave vial with a magnetic stirring bar. The vial was sealed with a cap and then purged with nitrogen to remove the oxygen (3X). Degassed and anhydrous toluene was added (C = 0.2 mol.L^{-1}, 0.4 mL) and the microwave vial was heated at 120 °C using a slow temperature ramp. After heating for 16 hours, 0.2 mL of degassed and anhydrous toluene was added. Four hours later the reaction was cooled to 65 ºC and then 1 ml of TCB was added. The mixture was poured in methanol/acidified water (10 % HCl; 9:1 ratio), and the solid was recovered by filtration using a 0.45 µm nylon filter. The polymer was washed using a Soxhlet apparatus with acetone, hexanes, dichloromethane and then chloroform. The chloroform fraction was reduced to 5-10 mL and then poured in methanol. The polymer was recovered by filtration over a 0.45 µm nylon filter and dry under vacuum (Y = 73%).

2.7.2 Synthesis of P3: M1 (0.167 mmol, 1eq.), **M2** (0.167 mmol, 1eq.), Pd_2dba_3 (4 % mol), tris(2-cycloheptyloxyphenyl)phosphine (BuraPhos) (20 % mol), K_2CO_3 (40 eq.) and pivalic acid (1eq.) were put in a microwave vial with a magnetic stirring bar. The vial was sealed with a cap and then purged with nitrogen to remove the oxygen (3X). Degassed and anhydrous THF was added (C = 0.1 $mol.L^{-1}$, 1.7 mL) and the reaction was heated with an oil bath pre-heated at 120 °C (reaction under pressure) until gelation of the reaction mixture. The reaction was cooled to 65 °C and then 1 ml of TCB was added. The mixture was poured in methanol/acidified water (10 % HCl; 9:1 ratio), and the solid was recovered by filtration using a 0.45 µm nylon filter. The polymer was washed using a Soxhlet apparatus with acetone, hexanes, and then chloroform. The chloroform fraction was reduced to 5-10 mL and then poured in methanol. The polymer was recovered by filtration over a 0.45 µm nylon filter and dry under vacuum (Y = 91%).

2.7.3 Synthesis of P4: M1 (0.131 mmol, 1eq.), **M5** (0.131 mmol, 1eq.), $P(OAc)_2$ (4 % mol), tris(2-methoxyphenyl)phosphine (16 % mol), Cs_2CO_3 (3 eq.) and pivalic acid (1 eq.) were put in a microwave vial with a magnetic stirring bar. The vial was sealed with a cap and then purged with nitrogen to remove the oxygen (3X). Degassed and anhydrous THF was added (C = 0.1 $mol.L^{-1}$, 1.3 mL) and the reaction was heated with an oil bath pre-heated at 100 °C (reaction under pressure) until gelation of the reaction mixture. The reaction was cooled to 65 °C and then 1 mL of TCB was added. The mixture was poured in methanol/acidified water (10 % HCl) (9:1), and the solid was recovered by filtration using a 0.45 µm nylon filter. The polymer was washed using a Soxhlet apparatus with acetone, hexanes, and then chlorobenzene. The chlorobenzene

fraction was reduced to 5-10 mL and then poured in methanol. The polymer was recovered by filtration over a 0.45 µm nylon filter and dry under vacuum (Y = 80%).

2.7.4 Synthesis of P5: M1 (0.139 mmol, 1eq.), **M5** (0.139 mmol, 1eq.), $P(OAc)_2$ (4 % mol), tris(2-cycloheptyloxyphenyl)phosphine (BuraPhos) (16 % mol), Cs_2CO_3 (3 eq.) and pivalic acid (1 eq.) were put in a microwave vial with a magnetic stirring bar. The vial was sealed with a cap and then purged with nitrogen to remove the oxygen (3X). Degassed and anhydrous THF was added (C = 0.1 $mol.L^{-1}$, 1.4 mL) and the reaction was heated with an oil bath pre-heated at 100 °C (reaction under pressure) until gelation of the reaction mixture. The reaction was cooled to 65 °C and then 1 mL of TCB was added. The mixture was poured in methanol/acidified water (10 % HCl) (9:1), and the solid was recovered by filtration using a 0.45 µm nylon filter. The polymer was washed using a Soxhlet apparatus with acetone, hexanes, and then chlorobenzene. The chlorobenzene fraction was reduced to 5-10 mL and then poured in methanol. The polymer was recovered by filtration over a 0.45 µm nylon filter and dry under vacuum (Y = 85%).

3. Results and discussion

3.1 Justification of the fluorination position on the thiophene moiety

As recently shown by Jiang *et al*., despite the similar size of fluorine and hydrogen atoms, the fluorination position on the phenyl group led to undesired torsion of the fluorinated diphenyl-DPP core [64]. While alkylated diphenyl-DPP core are known to be twisted and alkylated dithienyl-DPP are coplanar, one can think that the fluorination position on the thiophene ring would also affect the coplanarity of the resulting fluorinated dithenyl-DPP which can be detrimental for the electro-optical properties.

We then performed conformation analyses based on density functional theory to gauge the effect of both the amount and the position of fluorine atoms on the molecular structure of fDT-DPP (see Table S1 in ESI). The theoretical calculations revealed that when a fluorine atom is pointing towards the DPP core, the coplanarity is lost (**DPP-3-F**). On the other hand, the coplanarity of the fluorinated dithienyl-DPP is not affected when the fluorine atom is pointing away from the DPP core (**DPP-4-F**). Owing to these theoretical data, one can think that the synthesis of 4-fluoro-2-thiophenecarbonitrile (compound **6,** Scheme 2) would lead to coplanar fluorinated dithienyl-DPP moiety.

Recently, we have shown that theoretical calculations can also be used to rationalize and predict regio-selectivity of the direct heteroarylation polymerization [70, 71]. We performed a similar study using non-fluorinated DT-DPP moiety as reference to probe the effect of both different patterns on the activation energy (Gibbs free energy) of the C-H bond of the thiophene moiety in a catalytic direct heteroarylation polymerization. As shown in Figure 1, for **DPP**, a difference in the activation energy (ΔE_a) between H_α (24.2 kcal mol^{-1}) and H_β (29 kcal mol^{-1}) of 4.8 kcal mol^{-1} was calculated. Using Arrhenius's law it is possible to tentatively estimate a selectivity ratio of the α-position at 120°C (the temperature of polymerization). For this system, a ratio of about 450/1 favoring H_α can indeed be calculated for the **DPP** unit. Moreover, a difference in the activation energy (ΔE_a) between H_α and Hγ for **DPP** is found to be at 10.3 kcal mol^{-1} (24.2 kcal mol^{-1}vs 34.5 kcal mol^{-1}), giving a higher selectivity in favour of H_α (about 500000/1). For **DPP-3,4-F**, only one C-H bond is available for the concerted metalation-deprotonation (CMD) step in DHAP with an activation energy calculated at 19.4 kcal mol^{-1}. This lower activation energy value, compared to the activation energy of H_α of **DPP** (24.2 kcal mol^{-1}), shows the effect of electron withdrawing fluorine atom

on the adjacent C-H bond. For **DPP-3-F** a difference in the activation energy (ΔE_a) between H_α (23.5 kcal mol^{-1}) and H_β (25.5 kcal mol^{-1}) is only of 2.0 kcal mol^{-1}. Here, theoretical calculations show that the electron-withdrawing fluorine atom strongly modifies the activation energy of C-H_β bond (25.5 kcal $mol^{-1)}$ and has a small influence on the C-H_α (23.5 kcal mol^{-1}). Indeed, while the activation energy of H_α is 23.5 kcal mol^{-1} for **DPP-3-F**, the activation energy of H_β is lowered at 25.5 kcal mol^{-1} compared to 29 kcal mol^{-1} for **DPP** which lead to lower selectivity in favour of H_α (15/1) compared to 450/1 for **DPP**. Finally, **DPP-4-F,** activation energy of 19.8 kcal mol^{-1} for H_α and 30.1 kcal mol^{-1} for H_γ was calculated. In this case, the position of the fluorine atom on the flanking thiophene influences both H_α and H_γ. Indeed, when compared to **DPP,** activation energies are lowered (H_α 19.8 vs 24.2 kcal mol^{-1}; H_γ = 30.1 vs 34.5 kcal mol^{-1}). Although the activation energy of Hγ is decreased by 4.4 kcal mol^{-1} compared to **DPP**, a selectivity of about 500000/1 in favour of H_α over H_γ was calculated meaning that the polymerization reaction will likely proceed at the α-position and lead to well-defined copolymer. By combining the conformational analyses and the activation energy of each C-H bond, **DPP-4-F** derivatives would be the most useful fluorinated DPP core to obtain well-defined and coplanar conjugated polymer by DHAP.

3.2 Synthesis of monomers

On the basis of our previous work on fluorinated poly(3-alkylthiophene)s and fluorinated dithiophene-benzothiadiazole [71, 72], we decided to synthesize 3-bromo-2-(dimethyloctylsilyl)-thiophene (**2**) from lithiation of 2,3-dibromothiophene (**1**) in diethyl ether (at -80 °C) with *n*-BuLi followed by treatment with *n*-octyldimethylchlorosilane (Scheme 2). 3-Bromo-2-(dimethyloctylsilyl)-thiophene was

purified by vacuum distillation and obtained in 85% yield. Subsequent lithiation of **2** at -100 ºC in THF followed by a fast addition of NFSI *via cannula* provided 3-fluoro-2-(dimethyloctylsilyl)-thiophene (**3**) in 65 %. Unlike other fluoro-thiophene derivatives reported in the literature, which are purified using reverse phase chromatography, compound **3** was purified using silica gel. However, our synthetic procedure led to 3-fluoro-thiophene derivatives with traces of dehalogenated compound (2-(dimethyloctylsilyl)-thiophene) easily removed by normal phase chromatography. Freshly recrystallized NFSI, control of the reaction temperature (-100 ºC) and the use of TMEDA are mandatory to obtain **(3)** in a good yield. Lithiation of **3** with *n*-BuLi followed by quenching of the reaction with *N*,*N*-dimethylformamide led to 4-fluoro-5-(dimethyloctylsilyl)-2-thiophenecarboxaldehyde **(4)** in 85 %. Compound **4** was treated with an excess of tetrabutylammonium fluoride trihydrate (TBAF.3H_2O) in a mixture of THF/HCl at room temperature to afford pure 4-fluoro-2-thiophenecarboxaldehyde **(5)** in 85% yield. Treatment of **5** with hydroxylamine hydrochloride in NMP at 140°C followed by purification by column chromatography led to pure 4-fluoro-2-thiophenecarbonitrile **(6)** without any trace of 2-thiophenecarbonitrile, an unwanted by-product observed by El Kassmi *et al*. [73]. The purity of 4-fluoro-2-thiophenecarbonitrile is of paramount of importance for the next step that leads to the diketopyrrolopyrrole core with fluorinated flanking thiophene (fDT-DPP) (Scheme 3). Then, 3,6-(4-fluorothiophen-2-yl)pyrrolo[3,4-c]pyrrole-1,4-dione (**7**) was synthesized in one step by consecutive condensation of succinate ester with (**6**) in the presence of sodium alkoxide in 75%. In addition to the modification of the electronic properties of the DPP core, the fluorine atom installed on the 4-position on the flanking thiophene prevents β-branching and activates the C-H bond in α-position for DHAP. Alkylation

with either 1-bromodecane or 1-bromododecane led to **M5** and **M6** in 40% and 43% yields, respectively.

3.3 Synthesis and characterization of polymers

Fluorinated dithienyl-DPP-based copolymers were prepared by direct (hetero)arylation polymerization following guidelines found in our previous reports investigating reactivity [74] and selectivity [70] (Scheme 1). Non-fluorinated **P1** was already reported in literature [66]. In all cases, the polymerization reaction was stopped upon gelation of the reaction mixture. After precipitation in methanol, the polymers were purified by successive Soxhlet extractions. We found that the fluorine atom installed on the flanking thiophenes of the DPP moiety led to shorter polymerization times and enhancement of the molecular weights. As shown in Table 1, all the fluorinated copolymers have higher molecular weights compared to their non-fluorinated analogues. As an example, **P3** (Scheme 1) exhibits a number-average molecular weight of 44 kg mol^{-1} after 16 hours of reaction whereas, using the same polymerization conditions, **P4** has a number-average molecular weight 51 kg mol^{-1} obtained after only 30 min of reaction. Recently, we have shown that the use of bulky phosphine-based ligand can increase the selectivity of the DHAP while decreasing the unwanted homocoupling [70]. **P5** was synthesized using tris(2-cycloheptyloxyphenyl)phosphine (BuraPhos) instead of tris(2-methoxyphenyl)phosphine and number-average molecular weight up to 125 kg mol^{-1} was obtained after 30 min. Fluorinated dithienyl-DPP (fDT-DPP) pseudo-homopolymer (**P2**) was synthesized for OFET applications while fluorinated-DPP/carbazole copolymers (**P3**-**P5**) were synthesized for PSC applications.

Thermal properties were evaluated by thermal gravimetric analysis (TGA) and differential scanning calorimetry (DSC). All polymers exhibit good thermal stability

with 5% weight loss at temperature higher than 400 °C (see Table 1) while DSC traces did not revealed any thermal transition. NMR spectroscopy was useless to identify any β-branching or homocoupling within the conjugated backbone due to broad and featureless signals. Although a well resolved ^{1}H NMR spectrum was obtained for **P3** (TCE at 100°C, see ESI), the fluorinated analogues **P4** and **P5** exhibit strong aggregation and were barely soluble even in TCE at 100 °C.

A recently reported in the literature [66], the solid-state UV-Vis-NIR absorption spectrum of **P1** shows a maximum of absorption at 927 nm with a shoulder at 846 nm, for an optical bandgap of 1.17 eV. For **P2** (fluorinated analogue of **P1**), bathochromic shifts were observed for both the maximum of absorption (40 nm) and the shoulder (13 nm) (see Figure S40 in ESI). The optical bandgap taken from then onset of the absorption spectrum is 1.15 eV. An effect of the fluorine atom on the optical properties was also observed for **P3**-**P5** polymers in dilute chloroform solution (Figure 2). Indeed, a strong bathochromic shift (47 nm) of the maximum of absorption was observed for **P4** and **P5** (702 nm) compared to that of **P3** (655 nm). However, in the solid state, a bathochromic shift of 34 nm was observed for **P3** while no such behavior was found for **P4**-**P5** suggesting strong aggregation in solution. X-Ray diffraction analyses (powder) were also performed (see Figures S37-S39 in ESI). Typical d-spacing and lamellar distances for conjugated polymers were found for each fDT-DPP copolymer**.**

3.4. OFETs

To evaluate the semiconducting properties of **P2**, we prepared bottom-gate/bottom-contact (BGBC) OFET devices. All spin-coating processes were carried out under nitrogen, and the active channel layers were annealed at different temperatures for 20 min under nitrogen prior to measurements. OFET characteristics of the devices were measured under nitrogen conditions, and the field-effect mobility was extracted from the saturation regimes. **P2** displayed ambipolar properties and the device performance data are outlined in Table 2 and compared with previously reported **P1** [66]. Figure 3 shows the transfer and output characteristics of the BGBC devices based on **P2**. The output characteristics follow a typical trend exhibited by ambipolar devices where a super-linear increase in current is observed at low V_{GS} and high V_{DS}, which is due to the injection of the opposite charge carrier, and superposed standard saturation behavior with increasing V_{GS} for the dominate charge carrier. From the transfer characteristics, we observe V-shape I_{DS} patterns. As presented in Table 2, **P2** exhibited high mobilities with the maxima μ_h and μ_e where 0.80 $cm^2\ V^{-1}\ s^{-1}$ and 0.51 $cm^2\ V^{-1}\ s^{-1}$, respectively. The hole and electron mobilities are quite balanced with an average μ_e/μ_h of 0.68. In all cases, forward and backward scans in the transfer and output curves exhibited pronounced hysteresis of I_{DS}, which is frequently observed for OFETs due to trapping of the charge carriers in the gate dielectrics, at the interface of the active channel layer and dielectric, or in the active channel layer [75-77].

3.5 PSCs

As mentioned earlier, DPP-carbazole copolymers were investigated as electron donor in bulk heterojunction solar cells. Out-of-plan hole mobilities have been measured by using hole-only space-charge limited current (SCLC) devices (see Figure S41 in ESI). For pure polymer films, the hole mobilities are found to be slightly higher in fluorinated polymers ((1.9±0.3) x 10^{-4} and (2.3±0.4) x 10^{-4} cm^2 V^{-1} s^{-1} for **P4** and **P5**, respectively) compared to the non-fluorinated **P3** polymer ((5.0±1.0) x 10^{-5} cm^2 V^{-1} s^{-1}). These moderate mobility values are however sufficient to consider these polymers, and especially the fluorinated derivatives, as interesting electron-donor candidates in BHJ solar cells. **P3**-**P5** polymers have been characterized in blends with [6,6]-phenyl C_{71}-butyric acid methyl ester ($PC_{70}BM$) as electron-acceptor using an inverted device structure. The current density–voltage (J–V) characteristics of the solar cells measured under simulated AM 1.5G irradiation (with intensity of 100 mW cm^{-2}) are shown in Figure 4. The PSC parameters are summarized in Table 3. For both fluorinated polymers (**P4** and **P5**), using DIO as additive, the open-circuit voltage (V_{oc}) is slightly higher (by roughly 50 mV) than for the non-fluorinated polymers, in good agreement with the experimental HOMO energy levels reported in Table 1. The PCEs for fluorinated polymers are higher than those obtained for the non-fluorinated analogue. The best results are obtained for the high molecular weight polymer **P5**, with significantly larger short-circuit current densities (J_{sc}) and fill factors (*FF*). The average external quantum efficiencies (EQE), measured on the best-performing devices (Figure 5) follow the same trend. The J_{sc} values estimated from the EQE spectra are in-line with those measured under AM1.5 illumination. The noticeable difference in *FF* between non-fluorinated and fluorinated polymers correlates well with the higher out-of-plane mobility of **P4** and **P5**, which allows improved charge collection. Interestingly, the

polymer molecular weight turns out to have a dramatic impact on the solar cell performances despite its minor influence on the SCLC mobility. The increase in PCE is mostly due to the higher J_{sc} of **P5** based devices and to a slightly larger FF. This suggests that the molecular weight affects mostly the polymer/fullerene interface, at which charge generation occurs. The further PCE enhancement observed upon using a different additive (DPE versus DIO) supports this conclusion as the latter is expected to influence principally the blend morphology. The final maximum PCE of 7.42% is among the highest values reported so far for conjugated polymers prepared by direct heteroarylation polymerization.

Conclusion

In this study, we have developed an efficient synthetic procedure for the synthesis of new fluorinated dithienyl-DPP (fDT-DPP) monomers and copolymers. Two classes of conjugated copolymers have been prepared by direct heteroarylation polymerization (DHAP) and tested in OFETs and PSCs. We have shown that fluorinated DPP pseudo-homopolymer exhibits an ambipolar behavior in OFETs while fDT-DPP/carbazole copolymers show higher PCE than their non-fluorinated analogue. On the basis of these first examples, it is obvious that this new fDT-DPP moiety will lead to the development of new and high-performing materials for organic electronics devices.

Acknowledgements

The authors acknowledge the Natural Sciences and Engineering Research Council of Canada (NSERC), Université Laval (APOGÉE, Sentinelle Nord), the Canadian Institute for Advanced Research (CIFAR) and the European Fund for Regional Development (FEDER) within the framework of the program INTERREG V Rhin Supérieur and under the project n° 3.10 (PROOF) for their support. Compute Canada and Calcul Québec are also thanked for access to computational facilities. C. Roy is acknowledged for his help in the synthesis of some synthetic precursors.

References

1. Lu, L.; Zheng, T.; Wu, Q.; Schneider, A. M.; Zhao, D.; Yu, L. *Chem. Rev.* **2015**, *115***,** 12666-12731.

2. Etxebarria, I.; Ajuria, J.; Pacios, R.; *Org. Electron.* **2015**, *19***,** 34-60.

3. Sondergaard, R.; Hösel, M.; Angmo, D.; Larsen-Olsen, T. T.; Krebs, F. C. *Mater. Todays* **2012**, *15***,** 36-49.

4. Hösel, M.; Dam, H. F.; Krebs, F. C. *Energy Tech.* **2015**, *3***,** 293-301.

5. Tsai, P. T.; Tsai, C. Y.; Wang, C. M.; Chang, Y. F.; Meng, H. F.; Chen, Z. K.; Lin, H. W.; Zan, H. W.; Horng, S. F.; Lai, Y. C.; Yu, P. *Org. Electron*. **2014**, *15*, 893-903.

6. Berny, S.; Blouin, N.; Distler, A.; Egelhaaf, H. J.; Krompiec, M.; Lohr, A.; Lozman, O. R.; Morse, G. E.; Nanson, L.; Pron, A.; Sauermann, T.; Seidler, N.; Tierney, S.; Tiwana, P.; Wagner, M.; Wilson, H. *Adv. Sci.* **2016**, *3*, 1500342.

7. Zhang, S.; Ye, L.; Hou, J. *Adv. Energy Mater.* **2016**, *6*, 1502529.

8. Ouyang, X.; Peng, R.; Ai, L.; Zhang, X.; Ge, Z. *Nat. Photonics* **2015**, *9*, 520-525.

9. Zhou, H.; Zhang, Y.; Mai, C. K.; Collins, S. D.; Bazan, G. C.; Nguyen, T. Q.; Heeger, A. J. *Adv. Mater*. **2015**, *27*, 1767-1777.

10. Zhao, W.; Li, S.; Yao, H.; Zhang, S.; Zhang, Y.; Yang, B.; Hou, J. *J. Am. Chem. Soc*. **2017**, *139*, 7148-7151.

11. Kang, I.; Yun, H. J.; Chung, D. S.; Kwon, S. K.; Kim, Y. H. *J. Am. Chem. Soc.* **2013**, *135*, 14896-14899.

12. Yun, H. J.; Kang, S. J.; Xu, Y.; Kim, S. O.; Kim, Y. H.; Noh, Y. Y.; Kwon, S. K. *Adv. Mater.* **2014**, *26*, 7300-7307.

13. Choi, H.; Ko, S. J.; Kim, T.; Morin, P. O.; Walker, B.; Lee, B. H.; Leclerc, M.; Kim, J. Y.; Heeger, A. J. *Adv. Mater*. **2015**, *27*, 3318-3324.

14. Li, J.; Zhao, Y.; Tan, H. S.; Guo, Y.; Di, C. A.; Yu, G.; Liu, Y.; Lin, M.; Lim, S. H.; Zhou, Y.; Su, H.; Ong, B. S. *Sci. Rep.* **2012**, *2*, 754.

15. Farnum, D. G.; Mehta, G.; Moore, G. G. I.; Siegal, F. P. *Tetrahedron. Lett*. **1974**, *29*, 2549-2522.

16. Wallquist, O.; Lenz, R. *Macromol. Symp*. **2002**, *187*, 617-629.

17. Tieke, B.; Rabindranath, A. R.; Zhang, K.; Zhu, Y. *Beilstein J. Org. Chem*. **2010**, *6*, 830-845.

18. Qu, S.; Tian, H. *Chem. Commun*. **2012**, *48*, 3039-3051.

19. Chandran, D.; Lee, K. S. *Macromol. Res*. **2013**, *21*, 272-283.

20. Li, Y.; Sonar, P.; Murphy, L.; Hong, W. *Energy Environ. Sci*. **2013**, *6*, 1684-1710.

21. Naik, M. A.; Patil, S. *J. Polym. Sci. Part A: Polym. Chem*. **2013**, *51*, 4241-4260.

22. Nielsen, C. B.; Turbiez, M.; McCulloch, I. *Adv. Mater*. **2013**, *25*, 1859-1880.

23. Holliday, S.; Donaghey, J. E.; McCulloch, I. *Chem. Mater*. **2014**, *26*, 647-663.

24. Grzybowski, M.; Gryko, D. T. *Adv. Opt. Mater*. **2015**, *3*, 280-320.

25. Yi, Z.; Wang, S.; Liu, Y. *Adv. Mater.* **2015**, *27*, 3589-3606.

26. Jung, J. W.; Jo, J. W.; Jung, E. H.; Jo, W. H. *Org. Electron*. **2016**, *31*, 149-170.

27. Li, W.; Hendriks, K. H.; Wienk, M. M.; Janssen, R. A. J. *Acc. Chem. Res*. **2016**, *49*, 78-85.

28. Leclerc, N.; Chavez, P.; Ibraikulov, O. A.; Heiser, T.; Lévêque, P. *Polymers* **2016**, *8*, 11.

29. Liang, Y. Y.; Xu, Z.; Xia, J. B.; Tsai, S. T.; Wu, Y.; Li, G.; Ray, C.; Yu, L. P. *Adv. Mater*. **2010**, *22*, E135-E138.

30. Liao, S. H.; Jhuo, H. J.; Cheng, Y. S.; Chen, S. A. *Adv. Mater.* **2013**, *25*, 4766-4771.

31. Liu, Y.; Zhao, J.; Li, Z.; Mu, C.; Ma, W.; Hu, H.; Jiang, K.; Lin, H.; Ade, H.; Yan, H. *Nat. Commun*. **2014**, *5*, 5293-5301.

32. Nguyen, T. L.; Choi, H.; Ko, S. J.; Uddin, M. A.; Walker, B.; Yum, S.; Jeong, J. E.; Yun, M. H.; Shin, T. J.; Hwang, S.; Kim, J. Y.; Woo, H. Y. *Energy Environ. Sci*. **2014**, *7*, 3040-3051.

33. Meyer, F. *Prog. Polym. Sci*. **2015**, *47*, 70-91.

34. Chua, L. L.; Zaumseil, J.; Chang, J. F.; Ou, E. C. W.; Ho, P. K. H.; Sirringhaus, H.; Friend, R. H. *Nature* **2005**, *434*, 194–199.

35. Kim, F. S.; Ahmed, E.; Subramaniyan, S.; Jenekhe, S. A. *ACS Appl. Mater. Interfaces* **2010**, *2*, 2974–2977.

36. Bisri, S. Z.; Piliego, C.; Gao J.; Loi, M. A. *Adv. Mater.* **2014**, *26*, 1176–1199.

37. Irimia-Vladu, M.; Głowacki, E. D.; Troshin, P. A.; Schwabegger, G.; Leonat, L.; Susarova, D. K.; Krystal, O.; Ullah, M.; Kanbur, Y.; Bodea, M. A.; Razumov, V. F.; Sitter, H.; Bauer S.; Sariciftci, N. S. *Adv. Mater.* **2012**, *24*, 375–380.

38. Torricelli, F.; Ghittorelli, M.; Smits, E. C. P.; Roelofs, C. W. S.; Janssen, R. A. J.; Gelinck, G. H.; Kovács Vajna Z. M.; Cantatore, E. *Adv. Mater.* **2016**, *28*, 284–290.

39. Xue, J.; Li, C.; Xin, L.; Duan L.; Qiao, J. *Chem. Sci.* **2016**, *7*, 2888–2895.

40. Chapran, M.; Angioni, E.; Findlay, N. J.; Breig, B.; Cherpak, V.; Stakhira, P.; Tuttle, T.; Volyniuk, D.; Grazulevicius, J. V.; Nastishin, Y. A.; Lavrentovich O. D.; Skabara, P. J. *ACS Appl. Mater. Interfaces* **2017**, *9*, 4750–4757.

41. Jeong, H. G.; Khim, D.; Jung, E.; Yun, J. M.; Kim, J.; Ku, J.; Jang, Y. H.; Kim, D.Y. *J. Polym. Sci. Part A: Polym. Chem.* **2013**, *51*, 1029–1039.

42. Wang, Z.; Li, X.; Zou, Y.; Tan, J.; Fu, X.; Liu, J.; Xiao, C.; Dong, H.; Jiang, W.; Liu, F.; Zhen, Y.; Wang, Z.; Russell, T. P.; Hu, W. *J. Mater. Chem. C* **2016**, *4*, 7230–7240.

43. Chen, X.; Zhang, G.; Luo, H.; Li, Y.; Liu Z.; Zhang, D. *J. Mater. Chem. C* **2014**, *2*, 2869–2876.

44. Fukuta, S.; Wu, H. C.; Koganezawa, T.; Isshiki, Y.; Ueda, M.; Chen, W. C.; Higashihara, T. *J. Polym. Sci. Part A: Polym. Chem.* **2016**, *54*, 359–367.

45. Nakano, M.; Osaka, I.; Takimiya, K. *Macromolecules* **2015**, *48*, 576–584.

46. Zhou, X.; Ai, N.; Guo, Z. H.; Zhuang, F. D.; Jiang, Y.-S.; Wang, J. Y ; Pei, J. *Chem. Mater.* **2015**, *27*, 1815–1820.

47. Zhang, G.; Ye, Z.; Li, P.; Guo, J.; Wang, Q.; Tang, L.; Lu, H.; Qiu, L. *Polym. Chem.* **2015**, *6*, 3970–3978.

48. Wang, X.; Choi, H. H.; Zhang, G.; Ding, Y.; Lu, H.; Cho, K.; Qiu, L. *J. Mater. Chem. C* **2016**, *4*, 6391–6400.

49. He, Y.; Quinn, J.; Deng, Y.; Li, Y. *Org. Electron.* **2016**, *35*, 41–46.

50. Gao, Y.; Deng, Y.; Tian, H.; Zhang, J.; Yan, D.; Geng, Y.; Wang, F. *Adv. Mater.* **2017**, *29*, 1606217.

51. Yue, W.; He, T.; Stolte, M.; Gsänger, M.; Würthner, F. *Chem. Commun.*, **2013**, *50*, 545–547.

52. Yue, W.; Nikolka, M.; Xiao, M.; Sadhanala, A.; Nielsen, C. B.; White, A. J. P.; Chen, H. Y.; Onwubiko, A.; Sirringhaus, H.; McCulloch, I. *J. Mater. Chem. C* **2016**, *4*, 9704–9710.

53. Mukhopadhyay, T.; Puttaraju, B.; Senanayak, S. P.; Sadhanala, A.; Friend, R.; Faber, H. A.; Anthopoulos, T. D.; Salzner, U.; Meyer, A.; Patil, S. *ACS Appl. Mater. Interfaces* **2016**, *8*, 25415–25427.

54. Lin, G.; Qin, Y.; Zhang, J.; Guan, Y. S.; Xu, H.; Xu, W.; Zhu, D. *J. Mater. Chem. C* **2016**, *4*, 4470–4477.

55. Jiang, T.; Xue, Z.; Ford, M.; Shaw, J.; Cao, X.; Tao, Y.; Hu, Y.; Huang, W. *RSC Adv.* **2016**, *6*, 78720–78726.

56. Ji, Y.; Xiao, C.; Heintges, G. H. L.; Wu, Y.; Janssen, R. A. J.; Zhang, D.; Hu, W.; Wang, Z.; Li, W. *J. Polym. Sci. Part A: Polym. Chem.* **2016**, *54*, 34–38.

57. Shahid, M.; McCarthy-Ward, T.; Labram, J.; Rossbauer, S.; Domingo, E. B.; Watkins, S. E.; Stingelin, N.; Anthopoulos, T. D.; Heeney, M. *Chem. Sci.*, **2011**, *3*, 181–185.

58. Sun, B.; Hong, W.; Aziz, H.; Li, Y. *Polym. Chem.* **2015**, *6*, 938–945.

59. Chen, Z.; Gao, D.; Huang, J.; Mao, Z.; Zhang, W.; Yu, G. *ACS Appl. Mater. Interfaces* **2016**, *8*, 34725–34734.

60. Kim, J.; Han, A. R.; Hong, J.; Kim, G.; Lee, J.; Shin, T. J.; Oh, J. H.; Yang, C. *Chem. Mater.* **2014**, *26*, 4933–4942.

61. Gsänger, M.; Bialas, D.; Huang, L.; Stolte, M.; Würthner, F. *Adv. Mater.* **2016**, *28*, 3615–3645.

62. Zhao, Y.; Guo, Y.; Liu, Y. *Adv. Mater.* **2013**, *25*, 5372–5391.

63. Lu, G.; Kong, X.; Ma, P.; Wang, K.; Chen, Y.; Jiang, J. *ACS Appl. Mater. Interfaces* **2016**, *8*, 6174–6182.

64. Jiang,; Du, C. C.; Li, M. J.; Gao, K.; Kou, L.; Chen, M.; Liu, F.; Russell, T. P.; Wang, H. *Polym. Chem*. **2016**, *7*, 3311-3324.

65. Thompson, B. C.; Kim, Y. G.; Reynolds, J. R. *Macromolecules* **2005**, *38*, 5359.

66. Pouliot, J. R.; Sun, B.; Leduc, M.; Najari, A.; Li, Y.; Leclerc. M. *Polym. Chem*. **2015**, *6*, 278-282.

67. Blouin, N.; Michaud, A.; Gendron, D.; Wakim, S.; Plesu, R.; Belletête, M.; Durocher, G.; Tao, Y.; Leclerc, M. *J. Am. Chem. Soc*. **2008**, *130*, 732-742.

68. Zou, Y.; Gendron, D.; Aïch, B. R.; Najari, A.; Tao, Y.; Leclerc, M. *Macromolecules* **2009**, *42*, 2891-2894.

69. Ha, J. S.; Kim, K. H.; Choi, D. H. *J. Am. Chem. Soc*. **2011**, *133*, 10364-10367.

70. Bura, T.; Beaupré, S.; Légaré, M. A.; Quinn, J.; Rochette, E.; Blaskovits, J. T.; Fontaine, F. G.; Pron, A.; Li, Y.; Leclerc, M. *Chem. Sci*. **2017**, *8*, 3913-3925.

71. Roy, C.; Bura, T.; Beaupré, S.; Légaré, M. A.; Sun, J.-P; Hill, I. G.; Leclerc, M. *Macromolecules*, **2017**, accepted, ma-2017-00905u.R1

72. Blaskovits, J. T.; Bura, T.; Beaupré, S.; Lopez, S.; de Goes Soares, J.; Oh, A.; Quinn, J.; Li, Y.; Aspuru-Guzik, A.; Leclerc, M. *Macromolecules* **2017**, *50*, 162-174.

73. El Kassmi, A.; Fache, F.; Lemaire, M. *Synth. Commun*. **1994**, *24*, 95-101.

74. Grenier, F.; Goudreau, K.; Leclerc, M. *J. Am. Chem. Soc.* **2017**, *139*, 2816-2824.

75. Tsai, T. D.; Chang, J. W.; Wen, T. C.; Guo, T. F. *Adv. Funct. Mater.* **2013**, *23*, 4206-4214.

76. Ucurum, C.; Goebel, H.; Yildirim, F. A.; Bauhofer, W.; Krautschneider, W. *J. Appl. Phys.* **2008**, *104*, 084501.

77. Egginger, M.; Bauer, S.; Schwödiauer, R.; Neugebauer, H.; Sariciftci, N. S. *Monatsh Chem.* **2009**, *140*, 735-750.

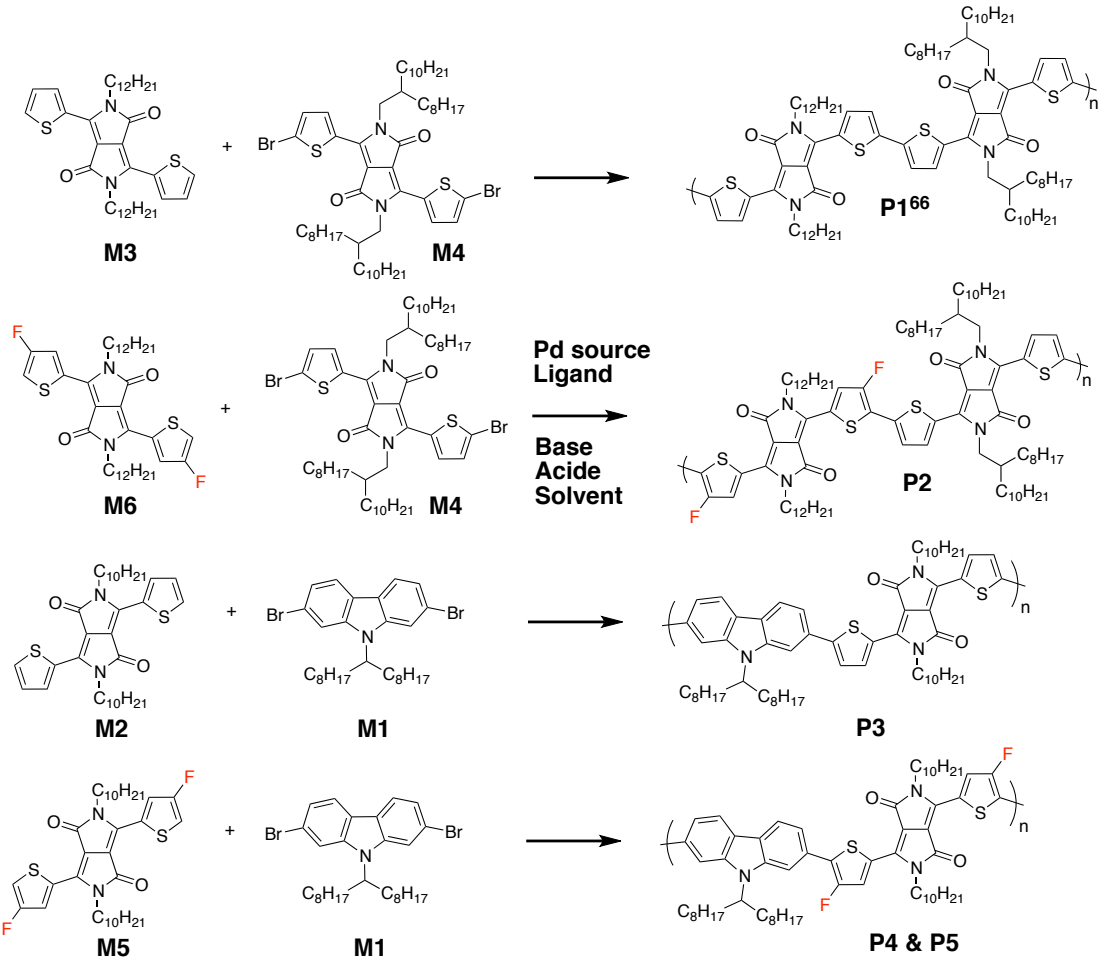

Scheme 1: Monomers and polymers investigated in this work.

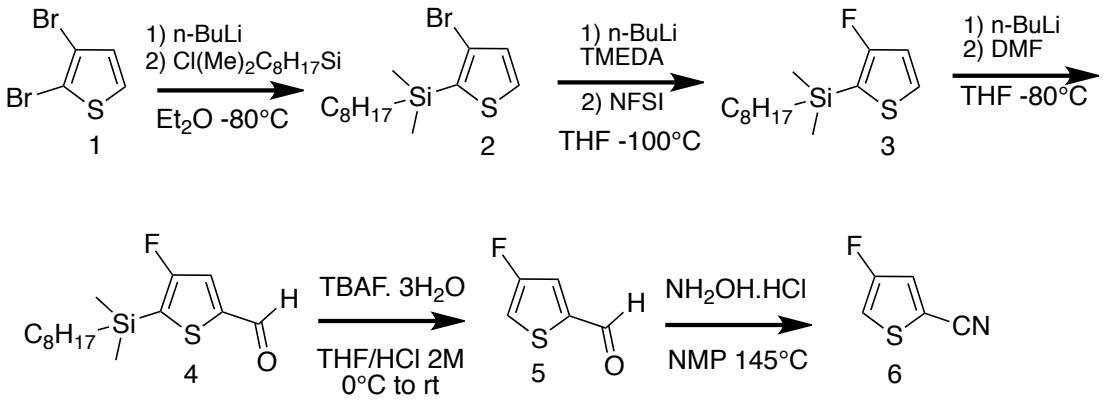

Scheme 2: Synthetic pathway for synthesis of 4-fluoro-2-thiophenecarbonitrile.

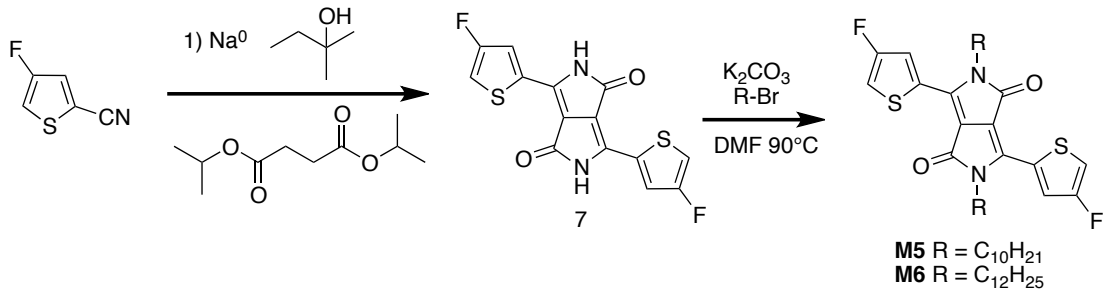

Scheme 3: Synthetic pathway for synthesis of monomers **M5** and **M6**.

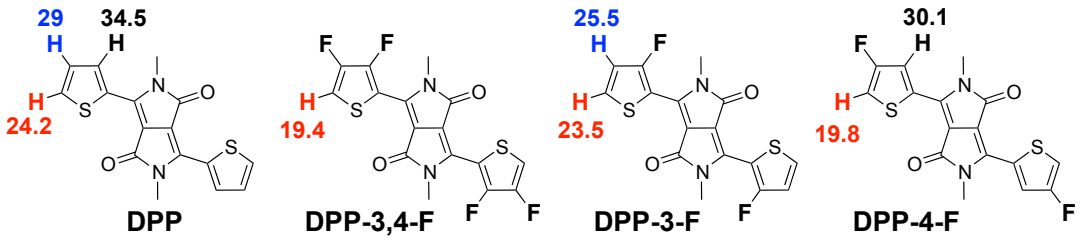

Figure 1. Computationally calculated Gibbs free energy of the CMD transition state associated to the transition state for the C-H bond cleavage at the α, β and γ positions.

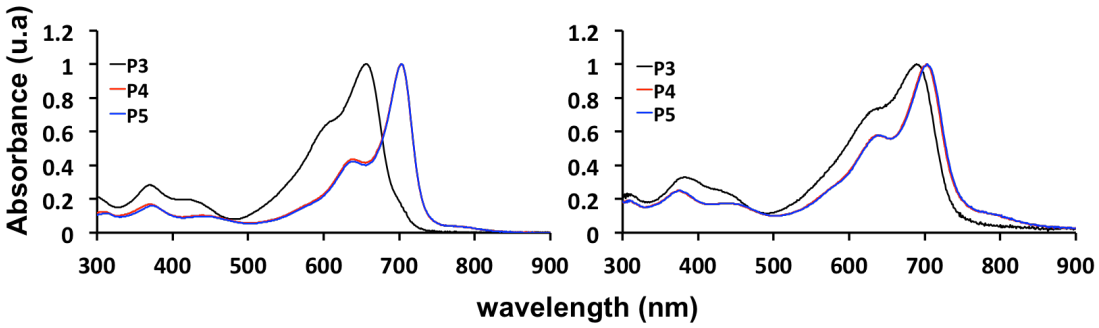

Figure 2. UV-Visible absorption spectra of **P3**-**P5** in solution in $CHCl_3$ (left) and in the solid state (right).

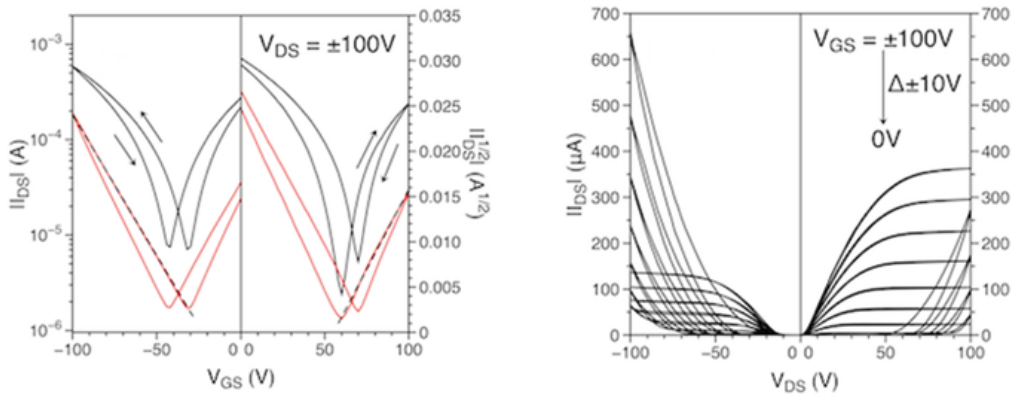

Figure 3**.** Transfer (left) and output (right) characteristics of a typical BGBC OFET device with **P2** as the channel semiconductor, which show ambipolar behavior. The **P2** film was annealed at 100 °C for 20 min in nitrogen.

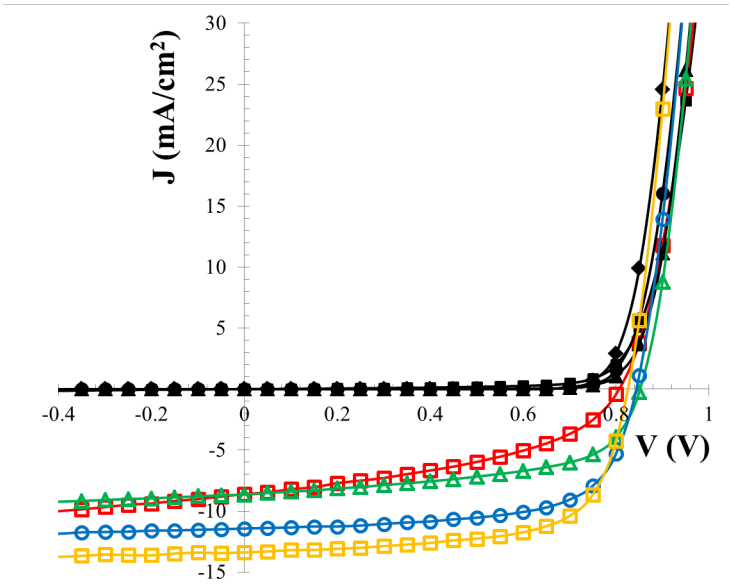

Figure 4. (*J-V*) characteristics measured in the dark (closed symbols) and under standard (AM1.5G 100 mW/cm2) conditions (open symbols) for **P3** (squares), **P4** (triangles), **P5** with DIO (circles) and **P5** with DPE (diamonds).

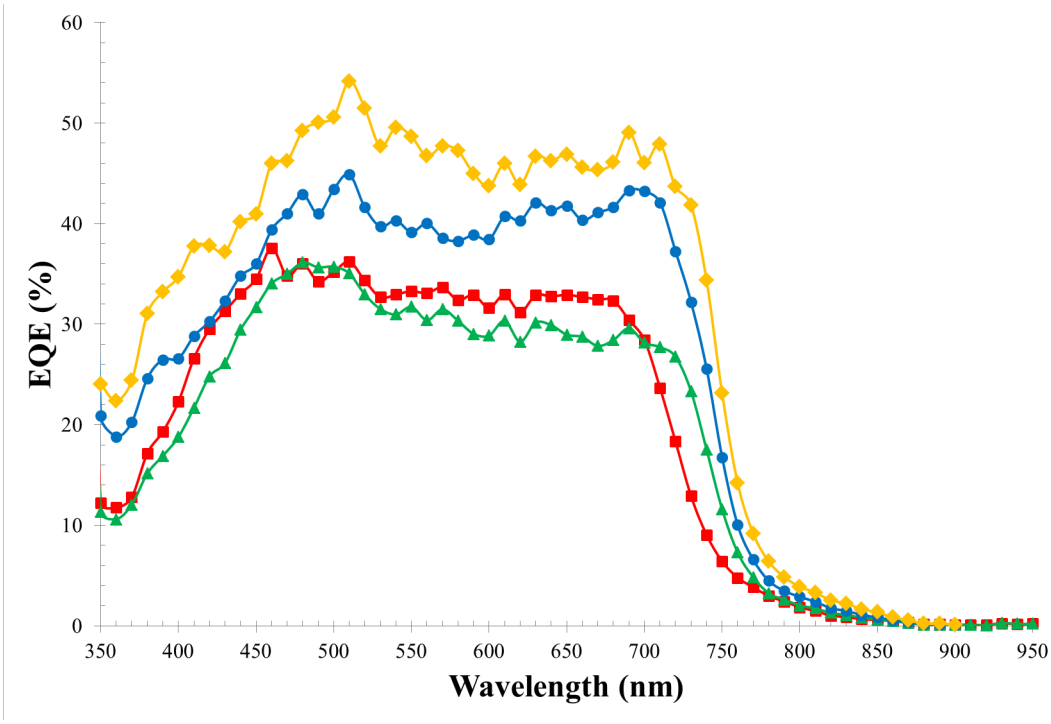

Figure 5. External quantum efficiency measured for **P3** (squares), **P4** (triangles) **P5** with DIO (circles) and **P5** with DPE (diamonds).

Table 1. Properties of polymers.

Entry	$\overline{M_n}$	Đ	Yield	HOMO	LUMO	λ max Abs (nm)		E_g^{opt}	TGA
						solution	Thin film		
	kg mol^{-1}		%	eV	eV	nm	nm	eV	°C
P1[66]	16	2.4	93	-5.45	-4.14	820/920	846/927	1.17	n.a
P2	22	3.0	73	-5.71	-4.04	887/962	859/967	1.15	430
P3	44	3.0	91	-5.46	-3.82	622/655	630/689	1.68	420
P4	51	3.7	90	-5.68	-3.97	639/702	639/702	1.65	420
P5	125	3.0	85	-5.68	-3.97	639/702	639/702	1.65	420

Table 2. OFETs performances

	p-channel		n-channel	
	μ_h[a] (cm^2 V^{-1} s^{-1})	I_{on}/I_{off}[b]	μ_e[a] (cm^2 V^{-1} s^{-1})	I_{on}/I_{off}[b]
P1[66]	0.22[d]	10^3	0.19[e]	n.a
P2	0.80[d] (0.73)	10^3	0.51[d] (0.50)	10^2

[a]Maximum mobilities measured under nitrogen in saturated regime. The average values are in brackets. [b]Current on/off ratio. [c]Calculated from the average mobilities. [d] Bottom Gate Bottom Contact configuration (BGBC), where the **P2** films were annealed at 100 °C for 20 min in nitrogen. [e]Top Gate Bottom Contact configuration (TGBC).

Table 3. Best photovoltaic parameters measured with different polymers

Polymer	Additive	V_{oc}	J_{sc}	FF	PCE
		mV	mA/cm^2	%	%
P3	DIO	807	8.63	44.1	3.07 (3.0)
P4	DIO	854	8.57	57.7	4.23 (4.1)
P5	DIO	845	11.4	65.9	6.37 (6.2)
P5	DPE	828	13.6	65.8	7.42 (7.3)

(Values in brackets are Average PCE values)